

Tailoring Spectral Response of Grating-Assisted Co-Directional Couplers with Weighting Techniques and Rational Transfer Functions: Theory and Experiment

Anatole Lupu

Centre de Nanosciences et de Nanotechnologies, CNRS, Université Paris-Saclay, C2N—10 Boulevard Thomas Gobert, 91120 Palaiseau, France; anatole.lupu@c2n.upsaclay.fr

1. Translation of CMT Model Into Opto-Geometric Design of Grating Assisted Directional Coupler

1.1. Initial Choices Regarding Grating Assisted Directional Coupler Material Platform

III-V semiconductors are currently the only materials that can simultaneously perform optical emission (laser), optical guidance (filter) and photoreception (pin photodiodes) functions. They are therefore perfectly suited to monolithic integration of circuits such as 1.3/1.3- μm or 1.3/1.5 μm diplexers.

The most commonly used substrates are of two types: InP and GaAs. Only materials epitaxially grown on InP can produce integrated circuits operating around 1.35 μm and 1.5 μm . We have therefore use materials epitaxially grown on InP.

The III-V lattice-matched alloys on InP substrate are either of InGaAsP type (phosphorus process) or InGaAlAs type (aluminium process). The phosphorus process was chosen because it currently allows the production of high-performance lasers, with well-controlled technology. The epitaxy technique used is atmospheric pressure organometallic vapor phase epitaxy (AP-MOCVD). This technique is well suited to the production of large surfaces. It allows excellent material quality to be obtained over large surfaces and therefore to manufacture low-loss waveguides [100]. The band gap wavelength λ_g then varies from 0.92 μm (1.35 eV) for InP to 1.65 μm (0.75 eV) for the InGaAs ternary [101]. We use $\text{In}_{1-x}\text{Ga}_x\text{As}_{1-y}\text{P}_y$ with $y \approx 0.22x$ respecting the lattice matching condition with the InP substrate.

In our application, the materials composing the grating assisted directional coupler (GADC) filter must be transparent at the working wavelength $\lambda \approx 1.3 \mu\text{m}$. We will typically use a quaternary InGaAsP alloy with electronic band gap wavelength $\lambda_g \approx 1.22 \mu\text{m}$. The materials used are intentionally undoped, which avoids high propagation losses due to free carriers [100,102].

Knowledge of the value of the refractive index $n(\lambda_g, \lambda)$ of the considered quaternary alloys is an essential element in the design of the component. We have chosen to use an analytical expression $n(x, \lambda)$ based on experimental measurements carried out by the Brewster angle method (precision on the value of the index of the order of 0.01) [32]. Figure S1 shows the refractive index values of the quaternary alloy ($\lambda_g \approx 1.22 \mu\text{m}$) as a function of the working wavelength λ . These refractive index values of the quaternary alloy form the basis of our modeling.

Received: 31 October 2024

Revised: 31 December 2024

Accepted: 7 January 2025

Published: 15 January 2025

Citation: Lupu, A. Tailoring Spectral Response of Grating-Assisted Co-Directional Couplers with Weighting Techniques and Rational Transfer Functions: Theory and Experiment. *Photonics* **2025**, *12*, 73. <https://doi.org/10.3390/photonics12010073>

Copyright: © 2025 by the authors. Submitted for possible open access publication under the terms and conditions of the Creative Commons Attribution (CC BY) license (<https://creativecommons.org/licenses/by/4.0/>).

As detailed in the main body of the paper, the chosen filter structure is a horizontal asymmetric directional coupler. The two critical points that need to be solved for this type of filter are the achievement of isotropy in TE, TM polarizations and the reduction of side-lobes. It has been shown that coupled mode theory (CMT) allows to adequately model this type of object in order to obtain the desired spectral response. The essential parameters that determine the spectral response of a coupler are the target filter central wavelength λ_0 , the dispersion with wavelength of the effective indices of the waveguides - $\delta(\lambda) = (\beta_1 - \beta_2)/2 = 2\pi(n_{\text{eff}1} - n_{\text{eff}2})/\lambda$, the period of the grating - Λ , the number of periods - N and the spatial profile of the coupling coefficient $\kappa(z)$.

The question then is how to determine these values from the given parameters of an asymmetric directional coupler that are the geometry and composition of the waveguides, the amplitude of the grating h and the interwaveguides separation distance g , called gap in the following.

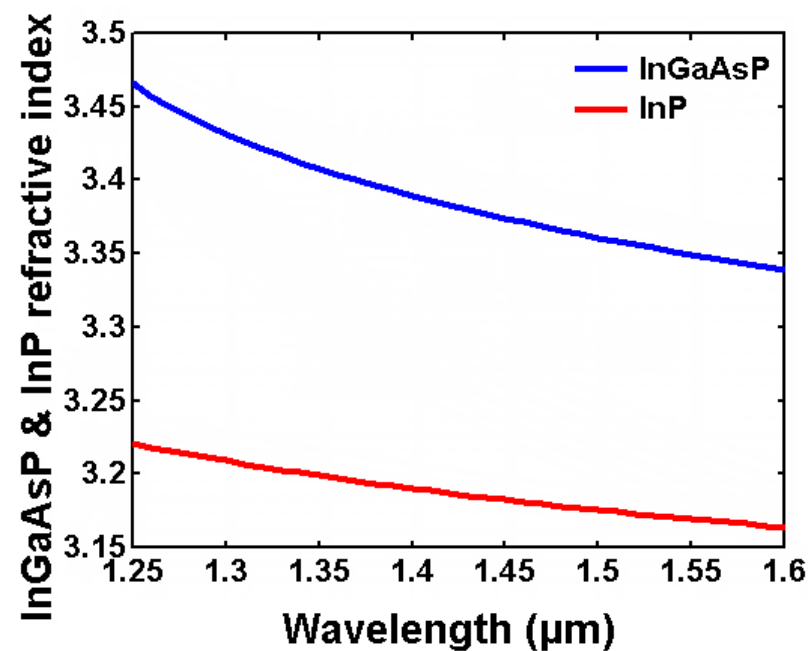


Figure S1. InP and InGaAsP ($\lambda_g \approx 1.22 \mu\text{m}$) refractive index as a function of wavelength.

The GADC chosen for the realization of the filter is composed of a slab-guiding layer loaded by two buried ridge waveguides. As it was shown in [41] such a coupler geometry allows to fulfill the polarization independence condition $\lambda_0^{\text{TE}} = \lambda_0^{\text{TM}}$. The schematic of the coupler cross-section is shown in Figure S2a. In order to facilitate the technological fabrication process the epitaxial heterostructure is composed of a thick $0.2 \mu\text{m}$ of quaternary InGaAsP slab layer and a series of bi-layers (BL) alternating InP and InGaAsP with a composition corresponding to $\lambda_g = 1.22 \mu\text{m}$.

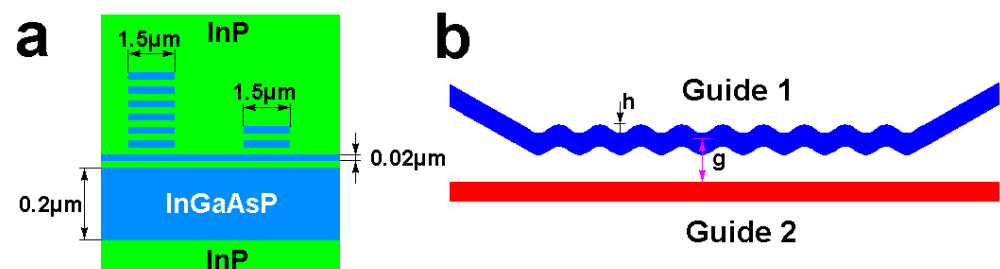


Figure S2. a) Schematic of GADC cut view. b) Sketch of a constant gap meander type GADC.

In order to increase the robustness of the central wavelength position λ_0 of the GADC with respect to fabrication imperfections, it is highly desirable to obtain a maximum asymmetry between the waveguides, i.e. a maximum difference between their effective index $\Delta n_{\text{eff}} = n_{1\text{eff}} - n_{2\text{eff}}$. This asymmetry is however limited by the single-mode condition of the considered waveguides. For this reason the waveguide ridge width w is fixed to $1.5 \mu\text{m}$. In this way, the waveguide with the highest effective index $n_{1\text{eff}}$ is close to the upper limit of the single-mode behavior and the waveguide with the lowest effective index $n_{2\text{eff}}$ is close to the lower limit of the single-mode domain. Although strictly speaking there is no lower cutoff in the mathematical sense of the term, in practice, below a certain waveguide dimension, the mode size becomes too large and is very sensitive to variations in geometric parameters due to technological manufacturing imperfections.

1.2. Determination of Directional Coupler Grating Parameters for Phase Matching Condition

The relation between the GADC central wavelength λ_0 , the grating period Λ and the waveguides index contrast $\Delta n_{\text{eff}} = n_{\text{eff}1} - n_{\text{eff}2}$ is given by the well-known relation [3,42,51,103]:

$$\Lambda = \lambda_0 / \Delta n_{\text{eff}} \quad (\text{S1})$$

The polarization independence condition imply in its turn that:

$$n_1^{\text{TE}} - n_2^{\text{TE}} = n_1^{\text{TM}} - n_2^{\text{TM}} \quad (\text{S2})$$

As a first approximation, the effective index of the waveguides can be calculated using many commercial mode solver software. In the present case, we used the multigrid finite difference mode solver BBV TempSelene. The distribution of the magnetic field component in the TE and TM polarizations for the two individual waveguides is shown in Figure S3. As can be seen, the confinement of the fundamental mode in the lateral X-axis direction is more significant for waveguide with higher ridge height. The mode intensity profile is very close to the Gaussian one with an overlap coefficient around 98%. The beam waist in the X-axis direction is about $1.2 \mu\text{m}$ and $1.6 \mu\text{m}$ for higher height ridge waveguide and lower height one, respectively. The confinement of modes in the Y-axis direction is not too different, however. This is confirmed by modes waist calculations, which is about $0.5 \mu\text{m}$ for Y-axis direction. Note also that the field distribution is essentially similar for TE and TM polarizations. The last point is particularly important to ensure that $\kappa_{\text{TE}} \approx \kappa_{\text{TM}}$ in order to achieve polarization independence in terms of the efficiency of light power transfer between the waveguides.

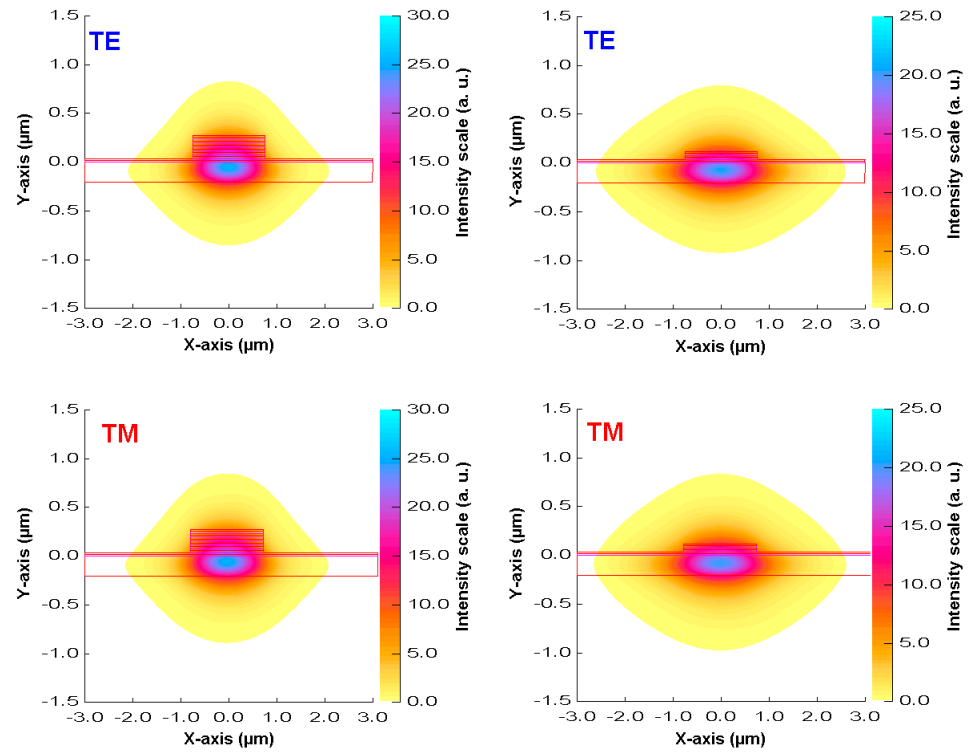


Figure S3. a) Waveguides cross-section view and fundamental mode magnetic field component intensity distribution (in linear scale a. u.).

The variation of the calculated effective index of the waveguides as a function of wavelength is shown in Figure S4a. As can be seen, in the wavelength region of interest, it follows a nearly linear relationship shown as an inset in Figure S4a. Given the well-known relationship between the phase refractive index and the group refractive index, it follows that the effective group index of the waveguide $n_{g\text{eff}}$ is nearly constant:

$$n_{g\text{eff}}(\lambda) = n_{\text{eff}}(\lambda) - \lambda \frac{dn_{\text{eff}}(\lambda)}{d\lambda} \quad (\text{S3})$$

The main parameters related to the effective index of waveguides are summarized in the Table 1. The waveguides index contrast Δn_{eff} in TE and TM polarizations, shown in Figure S4b, is a highly important parameter for the design of GADC. As can be seen, the crossing point of the $\Delta n_{\text{eff}}^{\text{TE}}$ and $\Delta n_{\text{eff}}^{\text{TM}}$ curves occurs at a wavelength $\approx 1.35 \mu\text{m}$. This is slightly different from the target central wavelength $\lambda_0 = 1.32 \mu\text{m}$ but the contrast difference $\Delta n_{\text{eff}}^{\text{TE}} - \Delta n_{\text{eff}}^{\text{TM}} \approx 10^{-4}$ is in practice quite negligible. It is two orders of magnitude smaller when compared to $\Delta n_{\text{eff}} = n_{\text{eff}1} - n_{\text{eff}2} \approx 10^{-2}$. The index contrast Δn_{eff} at the central wavelength $\lambda_0 = 1.32 \mu\text{m}$ corresponds approximately to a grating period $\Lambda = 126 \mu\text{m}$. This value of grating period will be refined in the next section by taking into account the influence of the coupling effect between the waveguides. Note also that the variation of index contrast Δn_{eff} with wavelength can be fitted with parabolic type equations presented in the inset of Figure S4b. The main parameters related to the waveguides index contrast Δn_{eff} are summarized in the Table 2.

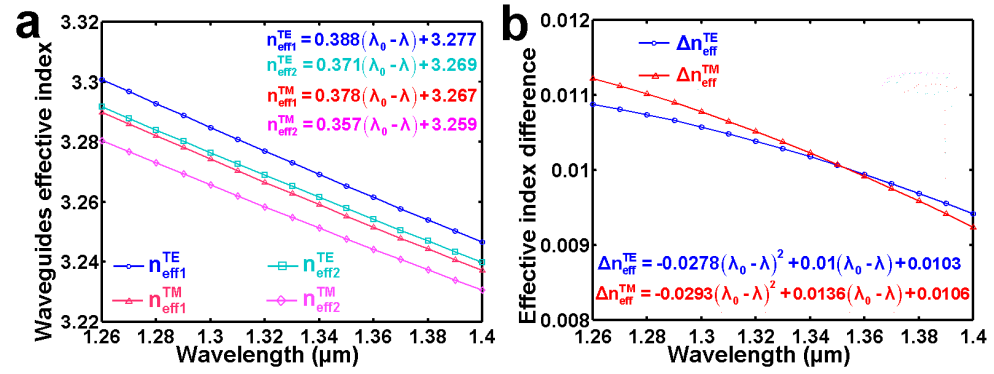


Figure S4. a) Wavelength dependence of the calculated effective index n_{eff} of two individual waveguides in TE and TM polarizations. b) Variation of the waveguides index contrast Δn_{eff} in TE and TM polarizations.

Table 1. Main parameters related to the effective index of waveguides.

Polarization	λ_0 (μm)	$n_{eff1}(\lambda_0)$	$dn_{eff1}/d\lambda$ (μm^{-1})	$n_{g\ eff1}$	$n_{eff2}(\lambda_0)$	$dn_{eff2}/d\lambda$ (μm^{-1})	$n_{g\ eff2}$
TE	1.32	3.277	0.388	3.789	3.267	0.371	3.756
TM	1.32	3.269	0.378	3.767	3.258	0.357	3.729

Table 2. Main parameters related to the waveguides index contrast Δn_{eff} .

Polarization	λ_0 (μm)	$\Delta n_{eff}(\lambda_0)$	$d\Delta n_{eff}/d\lambda$ (μm^{-1})	$d^2\Delta n_{eff}/(d\lambda)^2$ (μm^{-2})	L_c (mm)
TE	1.32	0.0103	0.01	-0.0278	2.37
TM	1.32	0.0106	0.0136	-0.0293	2.05

Another important parameter in the design of the phase matching grating is the amplitude of the grating corrugation h . For the realization of our filter we consider a meander type grating shown in Figure S2b. We now need to find a value of h compatible with the realization of the coupler. This can be done by taking into account the considerations related to the target $\Delta\lambda_{3dB} \approx 26$ nm bandwidth for an apodized GADC. The spectral response of an apodized GADC depends on both the coupling profile and the coupler length. For this reason, we consider a uniform GADC with constant gap. Since for the same coupler length, the $\Delta\lambda_{3dB}$ bandwidth of an apodized coupler is generally about 30% larger than that of a uniform coupler, we aim for the latter a bandwidth $\Delta\lambda_{3dB} \approx 18$ μm .

To find the GADC coupling length L_c fitting $\Delta\lambda_{3dB} = 18$ nm bandwidth, we can use the expression below derived in [20]:

$$\frac{\Delta\lambda_{3dB}}{\lambda_0} = \frac{0.8\Lambda}{L_c} \left[1 - \Lambda \left(\frac{\partial n_{eff1}}{\partial \lambda} - \frac{\partial n_{eff2}}{\partial \lambda} \right)_{\lambda=\lambda_0} \right]^{-1} \quad (S4)$$

Using elementary mathematical transformations, this expression can be cast in a more convenient form:

$$L_c = \frac{0.8\Lambda}{\Delta\lambda_{3dB}} \left[\frac{\lambda_0^2}{n_{g\ eff1} - n_{g\ eff2}} \right] \quad (S5)$$

The resulting coupling length is about 2.4 mm (exact values of L_c for TE and TM polarizations can be found in the Table 2). It is this value of $L_c = 2.4$ mm that was used for beam propagation method (BPM) simulations performed by BBV Prometheus software to optimize the grating amplitude using the following considerations.

As known, the coupling coefficient κ is proportional to the overlap integral of the two modes of the coupler and to the amplitude of the grating h [3,42,51,103]. If we now decrease the amplitude h , to keep the same value of the coupling coefficient, we must

increase the overlap of the modes of the coupler. Consequently, we must bring the waveguides closer together. In this case, it is necessary to check that the waveguides are not too close, because this can lead to technological difficulties in the implementation. This can also be detrimental for the rejection ratio, because of the coupling between the waveguides in the absence of the grating and the asymmetry of the spectral response, when a spatial variation $\kappa(z)$ is introduced, as it will be shown in the following section.

A value of amplitude h that is too large can also be detrimental, because of radiation losses for radii of curvature that are too small, but also because the grating could no longer be considered as a small perturbation. This will be detrimental for the rejection ratio. It is thus a question of finding a compromise between the extreme cases.

The empirically chosen amplitude of the grating is $0.5 \mu\text{m}$. The BPM simulations presented in the next section, used to refine the GADC design, show the absence of radiation losses for a grating with a reasonable interguides distance $g=2.6 \mu\text{m}$ for a coupling length of 2.45 mm .

1.3. Determination of Coupling Coefficient as Function of Coupler Interwaveguides Separation Distance

The next step is to validate the GADC waveguides structure design and determine the relation between the interwaveguides separation distance g and the coupling coefficient κ used in the CMT model. To this end we consider the following procedure based on BPM numerical simulations:

- Using BPM simulations, we find at the central wavelength $\lambda_0=1.32 \mu\text{m}$ the value of the gap between the waveguides as a function of the coupler length determined by an integer number of periods N and the grating period Λ . In practice, for a given number of GADC periods, we seek the value of g for which there is at least 20 dB of light intensity extinction for the bar-channel transmission and maximal $\approx 100\%$ intensity for the cross-channel transmission, as illustrated in Figure S5.

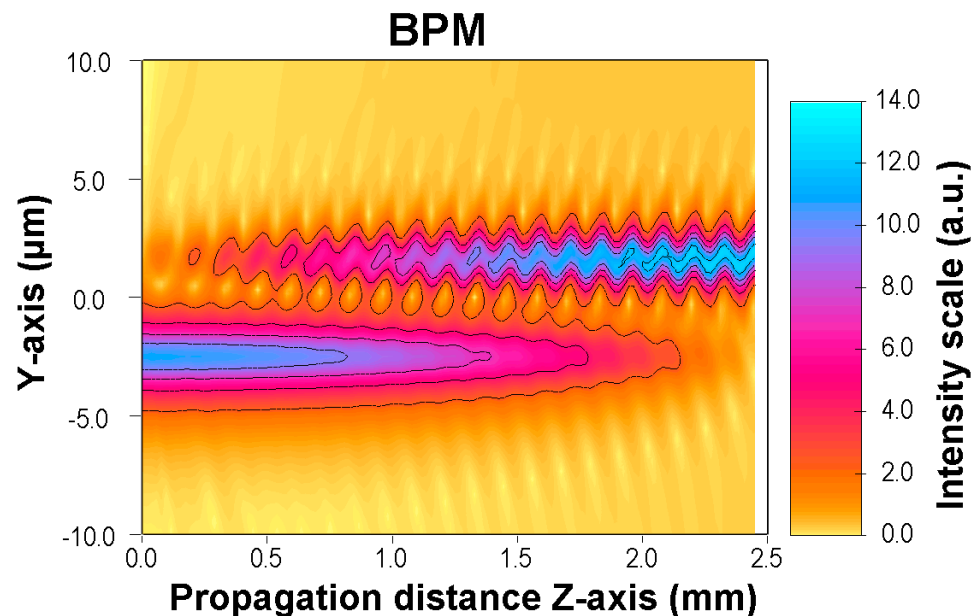


Figure S5. BPM simulation showing field intensity distribution for a 20 periods GADC at $\lambda_0=1.32 \mu\text{m}$.

- The resulting dependence of gap variation as function of GADC number of periods is shown in Figure S6a. To find the relation between the gap and the coupling coefficient, we can use the following expression (Equations 33 and 36 in Ref. [103]) that links κ to the GADC length expressed in an integer number of periods $L=N\Lambda$:

$$\tan(\pi/4N) = \kappa/\delta \quad (S6)$$

The resulting dependence $g(\kappa)$ is displayed in Figure S6b. This dependence $g(\kappa)$ can be approximated by the following analytical expression [26]:

$$g = g_0 + a \cdot \exp((\kappa_0 - \kappa)/s) \quad (S7)$$

By means of a fitting procedure we found the values of the coefficients entering this expression: $g_0 = 1.25 \mu\text{m}$, $a = 2.2 \mu\text{m}$, $\kappa_0 = 0.48 \cdot 10^{-3} \mu\text{m}^{-1}$, $s = 1.1 \cdot 10^{-3} \mu\text{m}^{-1}$. We see that g_0 which corresponds to $\kappa = +\infty$ determines the minimum distance between the waveguides. It is thus an indicator of technological feasibility.

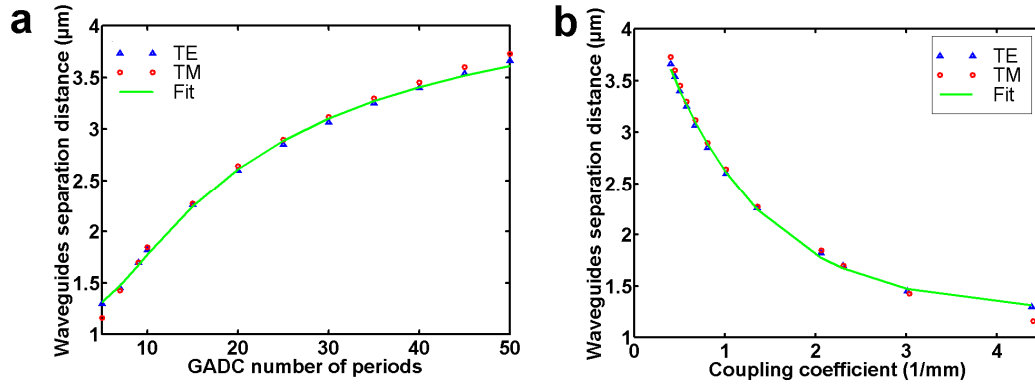


Figure S6. a) Interwaveguides separation distance variation as function of GADC number of periods b) Interwaveguides separation distance variation as function of coupling coefficient.

- Note that in order to maintain $\lambda_0 = 1.32 \mu\text{m}$, a fine-tuning of the grating period $\Lambda(g)$ is also required. This dependence is illustrated in Figure S7a. As can be seen, for low values of coupling coefficient $\kappa \leq 1 \text{ mm}^{-1}$ the grating period Λ is almost constant but notably decreases for higher values of κ . This result illustrates the importance of taking into account and compensating for the grating period chirp induced by the coupling between the waveguides. This chirp effect can be directly translated in a variation of the grating period length as a function of the interwaveguides separation distance, as illustrated in Figure S7b.

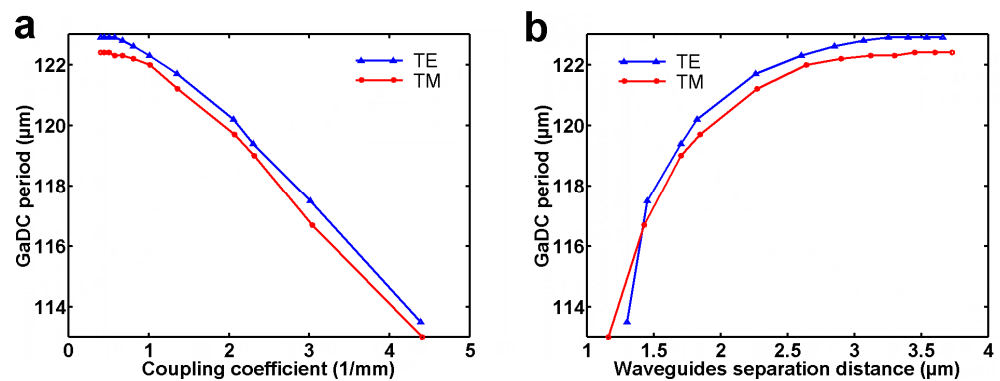


Figure S7. a) GADC period length Λ as function of coupling coefficient. b) GADC period length Λ as function of the separation distance.

1.4. Validation of GADC Design

We therefore have all the essential parameters which allow us to perform BPM modeling of the spectral behavior of a GADC. The simplest way to check the validity of such a modeling is to consider the case of a GADC with a constant coupling coefficient. To do this, let us take the case of a coupler composed of 20 sections with a grating period

$\Lambda=122.5\text{ }\mu\text{m}$. The resulting spectral response obtained by BPM simulations is shown in Figure S8.

As can be seen, BPM simulations show a $\Delta\lambda_{3\text{dB}}\approx 19\text{ }\mu\text{m}$ bandwidth for TM polarization and $\Delta\lambda_{3\text{dB}}=23\text{ nm}$ for TE. The bandwidth for TE is always wider since $d\Delta n_{\text{eff}}/d\lambda$ is lower. The polarization independence condition is fulfilled with a precision of 1 nm, that represents a very good result ($\lambda_0^{\text{TE}}=1.321\text{ }\mu\text{m}$, $\lambda_0^{\text{TM}}=1.322\text{ }\mu\text{m}$). The extinction ratio on the bar-channel is greater than 25 dB, which proves that the coupling coefficient and the interguides distance are correctly determined for this coupler.

Unlike the spectral response predicted by the basic CMT, we notice a pronounced asymmetry of the spectral response present in the BPM simulations. The level of the first secondary lobe on the short wavelength side is -12.5 dB , while on the long wavelength side it is -6.5 dB . It is worth noting that such asymmetry of the spectral response for a coupler with uniform interguides distance may be just an artifact related to insufficient accuracy of the BPM simulations.

To verify this point, a fabrication test with uniform gap GADCs was performed. To account for possible deviations of the experimental results from the modeling predictions, a series of GADCs with a grating period variation from $122.5\text{ }\mu\text{m}$ to $192.5\text{ }\mu\text{m}$ by steps of $5\text{ }\mu\text{m}$ and interguides distance $g=2.5\text{ }\mu\text{m}$ was implemented on the mask.

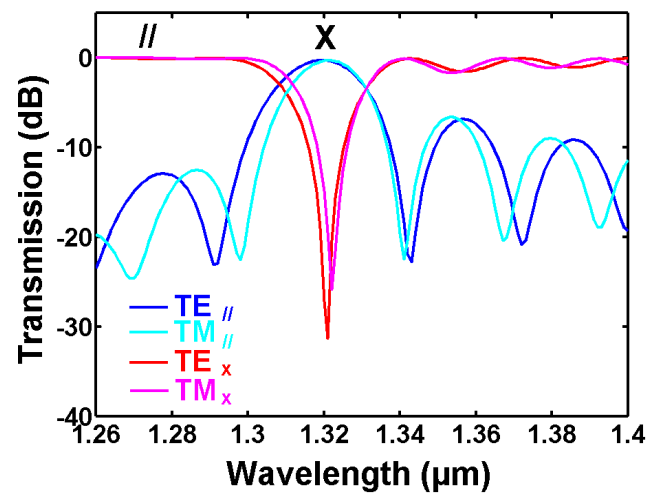


Figure S8. a) BPM numerical simulations of a GADC bar (//) and cross (X) channels spectral response in TE and TM polarizations.

The experimental spectra as well as the CMT modeling results for a GADC with grating period $\Lambda=122.5\text{ }\mu\text{m}$ are presented in Figure S9. It can be observed that the central wavelength polarization anisotropy is about 8 nm. The bandwidth is generally consistent with BPM simulations ($\Delta\lambda_{3\text{dB}}^{\text{TE}}=18\text{ nm}$ and $\Delta\lambda_{3\text{dB}}^{\text{TM}}=17\text{ nm}$). However, unlike BPM simulations, the asymmetry of the experimental spectral response is small. In contrast, the CMT modeling results show a good fit with the experimental results. The main waveguides parameters used for CMT modeling are summarized in the Table 3.

The CMT fitting procedure makes it possible to determine with precision the experimental value κ_{exp} of the coupling coefficient that is found to be about 38 % higher than the nominal value insuring $\approx 100\%$ light intensity transfer from the bar to the cross-channel. This fact leads us to think that the mode overlap calculated by BPM is not entirely correct. Therefore, the correspondence established in Section S1.3 between the coupling coefficient and the interguides distance is also not very exact. Nevertheless, it allowed us to estimate the necessary correction that was introduced in the next fabrication runs and allowed us to obtain correct results.

Table 3. Main parameters related to the waveguides index contrast Δn_{eff} .

Polarisation	λ_0 (μm)	$\Delta\lambda_{3\text{dB}}$ (nm)	Δn	$d\Delta n_{\text{eff}}/d\lambda$ (μm^{-1})	$d^2\Delta n_{\text{eff}}/(d\lambda)^2$ (μm^{-2})	κ_{exp} $10^{-3}\mu\text{m}^{-1}$	κ_{nom} $10^{-3}\mu\text{m}^{-1}$
TE	1.330	18	0.01100	0.013	0.015	1.30	0.996
TM	1.322	17	0.01082	0.015	0.040	1.35	0.975

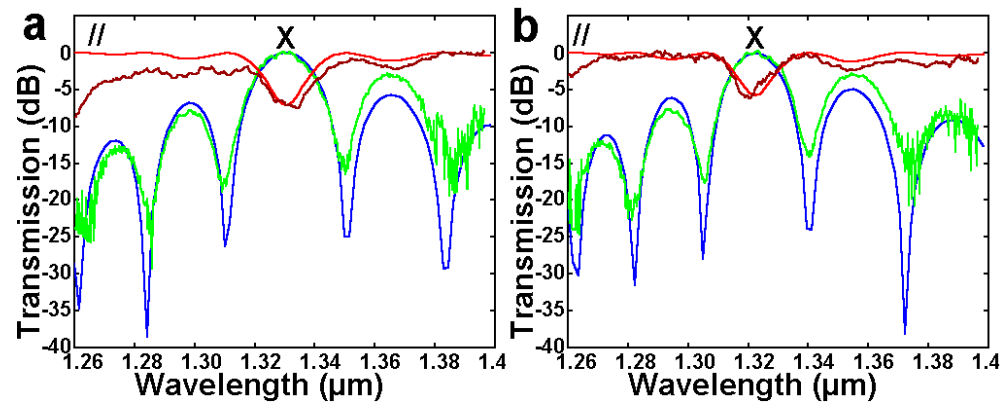


Figure S9. a) Experimental (brown and green curves) and CMT (red and blue curves) spectral response of a 20 periods ($\Lambda=122.5 \mu\text{m}$) GADC. a) TE polarization. b) TM polarization.

2. GADCs Fabrication Technology Process

The InGaAsP/InP layers are deposited by atmospheric pressure metal-organic chemical vapor deposition epitaxial process (AP-MOCVD). This currently well-known growth technique is not detailed here. With T-type rotating substrate reactor the epitaxy is carried out on 2-inch diameter InP substrates. On an epitaxial wafer, dispersions of $\pm 5 \text{ nm}$ around an average wavelength gap λ_g and dispersions of $\pm 5 \%$ on the thicknesses of the layers are typically obtained. The nominal values are obtained with an accuracy greater than 10 nm for λ_g and greater than $\pm 5 \%$ for the thicknesses.

Let us first recall the epitaxial heterostructure. It is composed, starting from the InP substrate (Figure S10):

- a layer of InP
- a thick layer ($0.2 \mu\text{m}$) of quaternary InGaAsP with $\lambda_g=1.22 \mu\text{m}$
- a series of bi-layers alternating InP and quaternary InGaAsP with $\lambda_g=1.22 \mu\text{m}$
- a last thin layer ($0.02 \mu\text{m}$) of InP

No layer is intentionally doped.

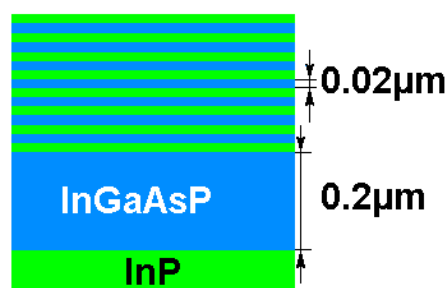


Figure S10. Schematic of the epitaxial heterostructure.

The transfer of the GADC mask patterns on the epitaxial wafer is performed by contact optical lithography and subsequent etching process. Most often, a silicon nitride mask provides better definition of the patterns and less under-etching. A PECVD (Plasma-Enhanced Chemical Vapor Deposition) silicon nitride layer acting as a hard mask for RIBE

(Reactive Ion Beam Etching) of InGaAsP/InP heterostructure is first of all deposited on the top of the wafer. This step is followed by photoresist layer deposition acting as a soft mask for silicon nitride RIE (Reactive Ion Etching) process.

The GADCs mask patterns are then transferred onto the photosensitive resist by UV exposure with a resolution limit of approximately 0.5 to 1 μm . We choose to produce patterns larger than 1.5 μm (width of the waveguides making up the coupler). Dimensional control of approximately $\pm 0.1 \mu\text{m}$ is possible using verniers (Figure S11). The alignment accuracy of one mask pattern over another is approximately 0.5 μm . These characteristics are valid in the case of flat structures (i.e. without marked relief), and therefore in the case of the coupler for which the maximum thickness of the ridge does not exceed 0.2 μm .

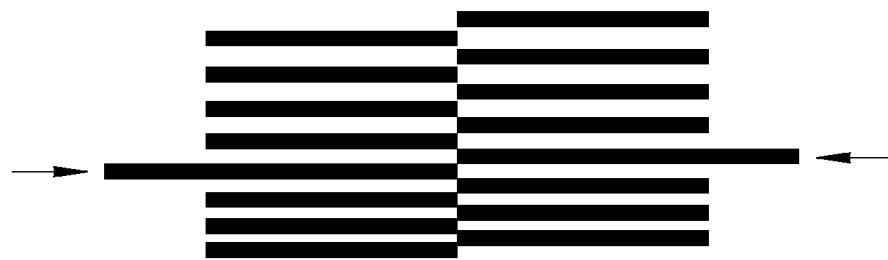


Figure S11. Vernier type test patterns for checking waveguide widths.

The etching processes used to transfer the silicon nitride mask patterns into the InGaAsP/InP heterostructure are of two types: dry etching and wet etching. RIBE is well suited to the fabrication of GADC and has the advantage of being very well controlled in the laboratory. For better control of the etching depth, the precision of which is generally of the order of 10 % to 20 %, thin layers of InP, called stop-layers, are used. They are not etched by the selective etching mixtures and therefore make it possible to stop the wet etching on a given epitaxial layer. The uniformity of the etching depth thus depends only on the homogeneity of the epitaxial heterostructure and is much more precise.

The different technological steps of the technological fabrication process are summarized in Figure S12. The schematic cross-section of the coupler composed of 2 BL of slab waveguide and ridges of respective thicknesses 2 BL and 6 BC is shown in Figure S2a. To avoid delicate alignment steps, the GADC, whose 1.5 μm wide waveguides are spaced approximately 2 μm apart, is made using a self-aligned method. Silicon nitride is used as a mask for defining the patterns of the GADC waveguides. Two lithography/etching steps are then necessary to produce the coupler.

The first step is to etch the coupler to a depth equal to that of the lowest ridge height (2BL). This is done by optical UV lithography (Figure S12a) followed by RIE and RIBE etching and subsequent wet etching to reliably control the process by stop-layers (Figure S12b).

The thickness asymmetry between the two waveguides is then obtained by removing through an additional lithography and RIE step the silicon nitride mask from the waveguide with the lowest target ridge height. The second waveguide of the coupler remains protected by a specially deposited photoresist mask. A second RIBE step followed by wet-etching is then performed, up to a depth equal to the difference between the thickness of the two guides (6 BL-2 BL=4 BL). This second etching process is illustrated in Figure S12c.

The final step is the burial of the GADC waveguide structure with a few microns of InP using the AP-MOCVD process (Figure S12d). The wafer with fabricated couplers is then thinned and cleaved.

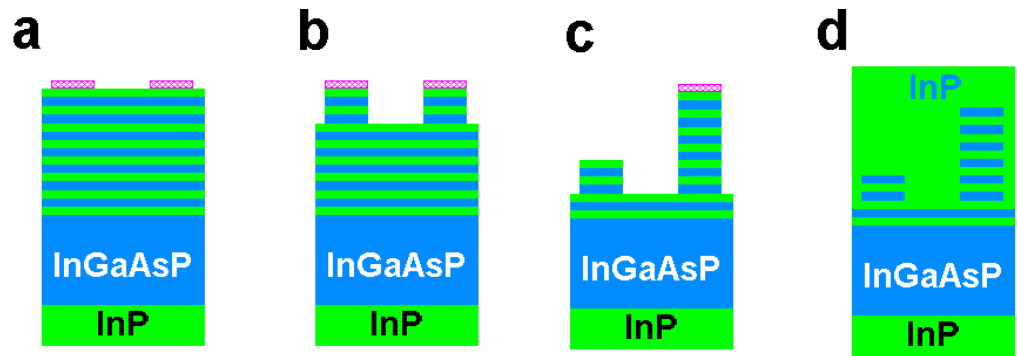


Figure S12. a) Definition of the silicon nitride etching mask for the GADC patterns. b) First etching step and definition of 2 BL thick waveguides coupler. c) Second UV lithography step with removal of the silicon nitride mask on one of the coupler waveguides followed by a second etching step of 4 BL depth. d) Burial of the GADC waveguide structure with a few microns of InP.

Throughout the coupler manufacturing process, rigorous control of critical dimensions is performed. The width of the waveguides is determined using verniers. Control of the etching thicknesses and the number of BL constituting the slab waveguide is done by SEM observations on control samples (Figure S13).

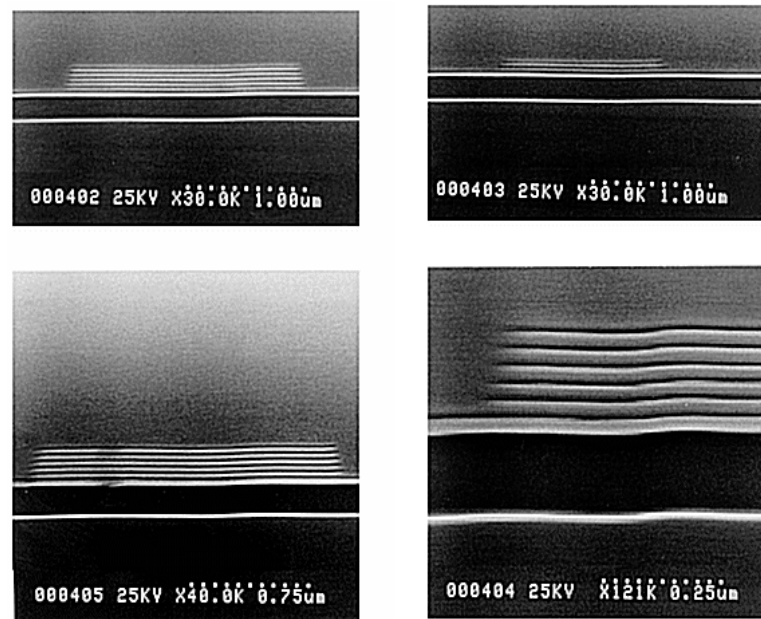


Figure S13. SEM micrographs of cleaved waveguides with different ridge height.

3. Optical Characterization of GADC Filters

The characterization of the GADC filters requires the use of a source covering a wide range of wavelengths. It is possible to use either a broadband source such as a light-emitting diode (LED) or a tunable laser. We chose to use a fiber-pigtailed LED because of a broader spectrum and a considerably shorter acquisition time of an HP71451A optical spectrum analyzer (OSA) compared to a TUNICS tunable laser. A temperature-stabilized LED, centered around 1.3 μm , emitting 34 μW at the output of a single-mode fiber was used for the filter measurements in a wavelength range extending from 1.2 μm up to 1.6 μm . For some measurements performed around 1.5 μm we used a tunable TUNICS laser that was forced to operate in spontaneous emission mode. The schematic of the optical bench setup is shown in Figure S14.

The light polarization state is controlled by using a pigtailed OFR polarization controller connected with TECOS “panda type” polarization maintaining (PM) lensed fiber with 2 μm focusing waist. A prior identification of the axes of the PM fiber makes it possible to establish a correspondence between the position of the polarizer and the TE and TM polarizations specific to the component. The orientation precision of the polarizer is $\approx 3^\circ$ and the polarization separation ratio is greater than 20dB.

The Elliot Martock optical coupling bench is used to inject light from the lens fiber into the optical waveguide. An optical microscope with long focal distance objectives is used to facilitate fiber alignment and select the GADC structure to measure. The light transmitted to the GADC output end is collected by a 32 \times long focal distance microscope objective with NA = 0.6. The collimated light is divided by a cube beam splitter toward Hamamatsu IR camera to visualize the waveguide mode and also transmitted to OSA used either as an optical power-meter or for spectral response characterization of GADCs in our study.

It should be noted that to reduce fiber coupling insertion losses, it is more advantageous to perform light injection into the less confined straight waveguide not bearing a grating. Further reduction of insertion losses can be achieved by considering various optical mode transformation techniques [104–108].

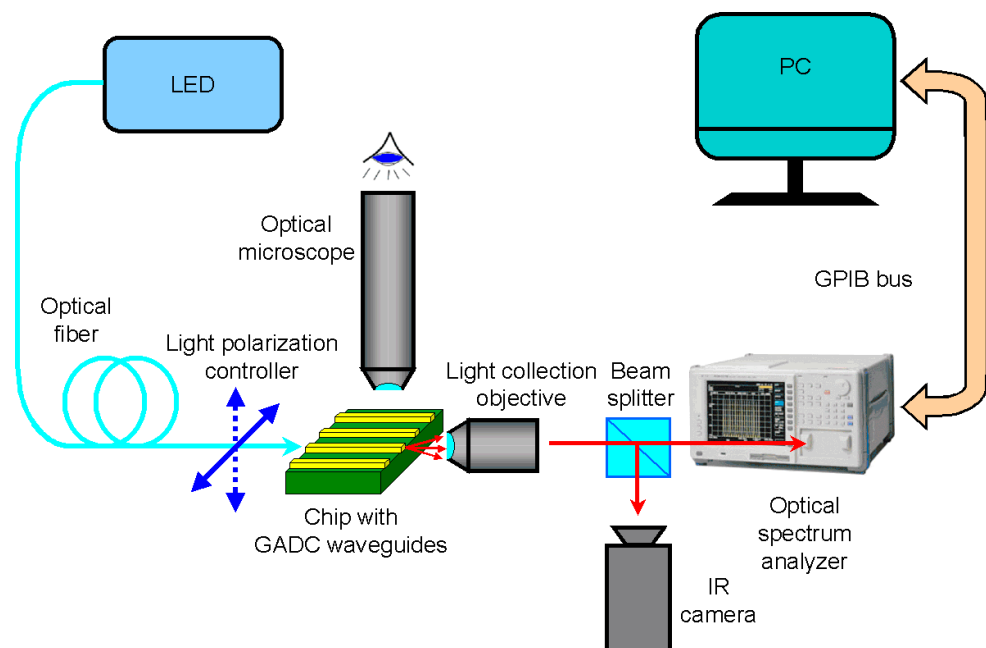


Figure S14. Schematic of the optical bench setup used for transmission spectra characterization.

Data Availability Statement: Data underlying the results presented in this paper are not publicly available at this time but may be obtained from the author upon reasonable request.

Conflicts of Interest: The author declares no conflicts of interest

Disclaimer/Publisher’s Note: The statements, opinions and data contained in all publications are solely those of the individual author(s) and contributor(s) and not of MDPI and/or the editor(s). MDPI and/or the editor(s) disclaim responsibility for any injury to people or property resulting from any ideas, methods, instructions or products referred to in the content.